

Probabilistic evaluation of concrete freeze-thaw design guidance

Scott H. Smith · Kimberly E. Kurtis  · Iris Tien

Received: 3 April 2018 / Accepted: 14 September 2018
© RILEM 2018

Abstract A novel limit-state function using Powers' models is developed to assess current freeze-thaw exposure categories and design criteria for concrete placements established by American, Canadian, and European standards organizations. Based upon performance assessments by standardized accelerated testing, the current specifications are shown to provide sufficient levels of reliability pending an appropriate mean air-void spacing factor. Sensitivity assessments of the model demonstrate that the spacing factor, saturation state, permeability, and freezing rate significantly influence the response of the air-entrained concrete. The model is validated with a large dataset derived from standard freeze-thaw tests, and an equation is developed to probabilistically design concrete for freeze-thaw resistance.

Keywords Freezing-and-thawing · Durability · Pore size distribution · Performance-based design

Abbreviations

FT	Freeze-thaw
ACI	American Concrete Institute
CSA	Canadian Standard Association
BS EN	British Standard European Norm
LS	Limit-state
DF	Durability factor
OPC	Ordinary Portland cement
<i>w/c</i>	Water-to-cement ratio
FORM	First order reliability method

1 Introduction

The response and resistance of concrete mixtures to freeze-thaw (FT) cycles has been studied since the early 1940s with major contributions by T.C. Powers. In the mid 1950s, P. Klieger conducted two studies [1, 2] relating the FT resistance of standard concrete mixtures to their respective 28-day compressive strength, water-to-cement ratio, and total air content. Despite significant advancements made in concrete technology (e.g., chemical admixtures, curing techniques, cement compositions), international durability requirements for concrete exposed to FT largely reflect the design variables and associated values

S. H. Smith
Georgia Institute of Technology, 790 Atlantic Drive NW,
Room 5132, Atlanta, GA 30318, USA
e-mail: ssmith314@gatech.edu

K. E. Kurtis (✉)
Georgia Institute of Technology, 790 Atlantic Drive NW,
Room 4154, Atlanta, GA 30318, USA
e-mail: kkurtis@gatech.edu

I. Tien
Georgia Institute of Technology, 790 Atlantic Drive NW,
Room 4140A, Atlanta, GA 30318, USA
e-mail: itien@ce.gatech.edu

measured by Klieger. More recently, the problem of ‘joint-rot’ in rigid pavements, advancements in imaging and experimental technologies, and improved mechanistic models have produced new understanding of damage mechanisms associated with FT [3–7]. Results of recent studies have widened the gap between research and practice, necessitating an examination of current design provisions, as specified in American (ACI), Canadian (CSA) and European (BS EN), standards to ensure FT performance [8–12]. The authors herein probabilistically examine the current exposure categories and design criteria established for FT resistance using models developed by T.C. Powers [13, 14] in a novel limit-state form.

Previous efforts to probabilistically evaluate or predict the FT resilience of concrete mixtures have utilized limited experimental datasets to inform ‘best-fit’ functions [15–18]. The utilization of Powers’ models advances previous work in two ways. First, the presented limit-state function is highly general (i.e., it can be utilized to assess mixtures across a broad range of physically relevant parameters). Second, the model’s limit-state form allows for the determination of reliability indices and sensitivity assessments familiar to the engineering community and germane to concrete design, production, and acceptance.

The intention of the presented work is to assess selected design variables—namely, compressive strength, total air content, and the ASTM C457 spacing factor—in the context of the developed limit-state function. Numerical findings are compared to published accelerated FT test results as in previous studies [7], where the use of the durability factor, DF, obtained from ASTM C666 testing provides a quantitative basis of comparison to probability of failure calculations.

Using the developed limit-state function, it is demonstrated how design variables can be quantitatively selected to ensure FT resistance. Additionally, analysis of the model allows for identification of model parameters that are not regularly considered, such as permeability and freezing rate, and examines their relative significance or importance. The presented model and findings encourage the movement away from the current prescriptive design criteria to performance-ensuring specifications based upon statistically informed and experimentally validated models.

2 Formulation and theory

2.1 General formulation and system of study

Limit-state (LS) models are composed of capacity and demand inputs that empirically generate regions of survival and failure for a system. Equation 1 and Fig. 1 detail how LS functions are generally developed and conceptualized [19]. In Eq. 1, $C(\mathbf{x})$ and $D(\mathbf{x})$ represent the capacity and demand functions where \mathbf{x} is a vector of explicit, random design variables. Figure 1 displays that failure occurs when the function, $LSF(\mathbf{x})$, is zero or negative, indicating the region where the demand, $D(\mathbf{x})$, placed on the system is equal to or exceeds the capacity, $C(\mathbf{x})$.

$$LSF(\mathbf{x}) = C(\mathbf{x}) - D(\mathbf{x}) \quad (1)$$

The presented LS function implements Powers’ models, detailed in subsequent sections, where the system under study is a single air void with a surrounding hardened paste shell, as detailed by Fig. 2. Although simplified, this model has been used to represent the critical region of air-entrained concrete where failure initializes [12]. The functions $C(\mathbf{x})$ and $D(\mathbf{x})$ take the form of the tensile strength of the hardened paste shell and the internal hydraulic pressure developed during a FT cycle, respectively. The air void system of the concrete and intrinsic properties of the hardened cement paste shell, such as the porosity and permeability, are modeled using Powers’ models due to their familiarity in the industry and research field [20, 21]. By using a physics-based model, the findings have inherent physical relevance

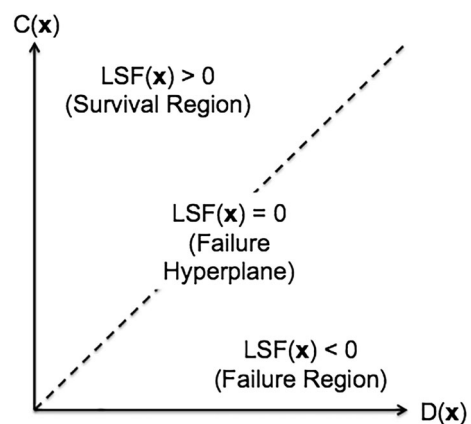


Fig. 1 Limit-state function schematic where the LS function hyper-plane separates the survival and failure regions

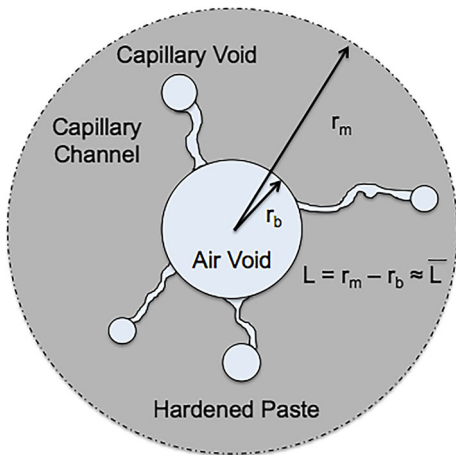


Fig. 2 The system of study contains a spherical air void with radius, r_b , and hardened paste shell of thickness, L

and can be readily interpreted to inform the design, placement, and response of a concrete mixture exposed to FT conditions.

2.2 Powers' hydraulic pressure theory

Powers' hydraulic pressure theory states that pressures are developed within the hydrated cement paste from the forced movement of pore solution due to volumetric expansion of freezing water [13]. The authors recognize that multiple other theories have been established since this time, such as those based upon Biot–Coussy theory [22]. For the purposes of this work, it is of interest to use the original model that describes the relationship between pressure development in the hardened cement paste and other environmental and material factors: freezing rate, distance between entrained air voids, and capillary saturation [21].

Powers' theory yields a closed form expression for the hydraulic pressure developed throughout the paste-shell surrounding an entrained air void of arbitrary size. Conservatively, the demand function, $D(\mathbf{x})$, is set to the maximal pressure developed over a distance, L , from the periphery of the air void and is displayed in Eq. 2. The values of viscosity, η , at 0 °C and the freezable water content per degree in the cement paste, U , are taken from Powers [13] as $1.9\text{e-}3$ Pa s and $2.34\text{e-}4$ kg °C⁻¹. R , the freezing rate, is defined by an allowable range specified in ASTM C666 [23], the capillary pore network, is assumed to be saturated,

$S_{cp} = 1$, and K is the permeability of the saturated hardened cement paste and is modeled as shown in Sect. 2.4 following [13, 14]. L and r_b represent the hardened cement paste shell thickness and the radius of the entrained air void shown in Fig. 2.

$$D(\mathbf{x}) = \frac{\eta}{3} \left(1.09 - \frac{1}{S_{cp}} \right) \frac{UR}{K} \left(\frac{L^3}{r_b} + \frac{3L^2}{2} \right) \quad (2)$$

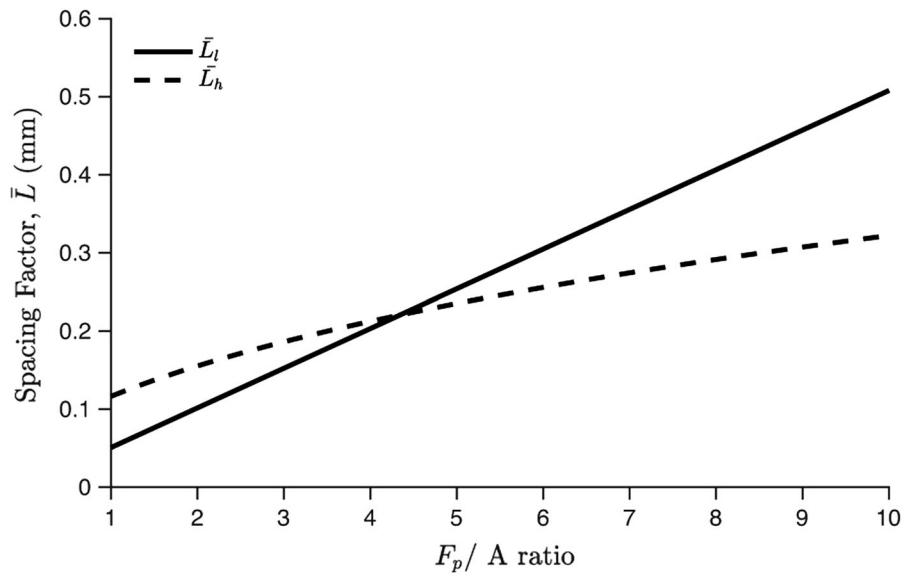
2.3 Air void systems

In addition to defining the hydraulic pressure theory in 1949, Powers also derived two spacing factor, \bar{L} , equations, which approximate half the distance between air voids, to ensure FT resistance for air-entrained concrete [13]. In his seminal work, the spacing factor is assumed to be an approximation of the thickness of the paste shell, L , displayed in Fig. 2 and Eq. 2. Powers' derivations are based upon approximations of the volumetric ratio of the cement paste, F_p , to the entrained air, A , where the radius of the air voids within the system is uniform. Within the original work, Powers states, "there is reason to believe that the factors obtained from either equation exceed the actual spacing [13]." Based upon this inclination, Powers substantiates the use of the lower value obtained from Eqs. 3 and 4, as shown in Fig. 3, for a given cement paste to entrained air volume ratio (F_p/A) and is reported as \bar{L} using standard ASTM C457 evaluation techniques.

Powers' first spacing factor, \bar{L}_1 , displayed in Eq. 3, is defined as the ratio of the volume of the cement paste to entrained air in the concrete multiplied by the quotient of the volume and the surface area for the uniform air void system. \bar{L}_1 is the applicable spacing factor for concretes with paste to entrained air (F_p/A) ratios less than 4.342 [13]. The second spacing factor, \bar{L}_h , displayed in Eq. 4, assumes that each air void is at the center of an equivalent cube of cement paste and the spacing factor adopts a geometric sense by approximating the value of the nearest distance from a corner of the idealized cube to the surface of the air void. \bar{L}_h is used for concretes with paste to entrained air (F_p/A) ratios greater than or equal to 4.342 [13].

$$\bar{L}_1 = \frac{r_b}{3} \left(\frac{F_p}{A} \right) \quad (3)$$

Fig. 3 Comparison plot of Powers' spacing factors for an arbitrary radius of 0.15 mm (0.006 in)



$$\bar{L}_h = r_b \left(1.4 \left(\frac{F_p}{A} + 1 \right)^{1/3} - 1 \right) \tag{4}$$

For the final LS function formulation, the spacing factor \bar{L}_h is utilized as the value of the shell thickness, L , found in Eq. 2. The use of \bar{L}_h is substantiated in two ways. First, \bar{L}_h is justified by its practicality in terms of concrete design (i.e., it is uncommon for (F_p/A) ratios to be less than 4.342 for mixtures that will be exposed to FT environments). For example, the mean (F_p/A) value for the concrete mixtures in the developed FT dataset, discussed in Sect. 3.1, is 8.8, indicating that \bar{L}_h is the spacing factor most often reported. Second, for (F_p/A) ratios greater than or equal to 4.342, \bar{L}_h gives a lower spacing factor than \bar{L}_l yielding smaller values of hydraulic pressure during freezing. Although smaller values of hydraulic pressure imply a reduction in likelihood of failure, due to the fact that \bar{L}_h is understood as an upper-bound for the “actual spacing” factor [13], it will yield more realistic approximations of the influence of freezing on the hardened cement paste shell. For the remainder of the paper, \bar{L}_h is assumed equivalent to L .

2.4 Intrinsic properties: porosity and permeability

Along with specifying a required compressive strength and total air content for a given FT exposure category, ACI, CSA, and BS EN codes also limit the water-to-cement ratio (w/c). The intent of the maximal limits

placed on the w/c is to reduce the amount of freezable water at early ages, which influences the final porosity of the cement paste and the overall permeability of the concrete [12]. Powers and Brownard’s model [14] for a cement paste’s capillary porosity, ϵ , which is a function of the w/c and degree of cement hydration (α_H), is employed to empirically model the permeability, K , found in Eq. 2 and published by Powers [13]. Equations 5 and 6 display the models used to determine the capillary porosity and the permeability of the hardened cement paste.

Although the w/c of a concrete mixture is specified under each provision for FT resistance, the value is maintained as a model input rather than a random design variable. The w/c is considered to be a mixture constant that has negligible variability as compared to parameters such as compressive strength, air content, and spacing factor. Additionally, the permeability of the hardened paste shell is considered to remain constant throughout the freezing cycle based upon Powers’ original discussion [13]. A future improvement of the presented model would consider the reduction in the hardened cement paste permeability as a function of the freezing temperature.

$$\epsilon = \frac{w/c}{w/c + \rho_w/\rho_c} - 1.32 \left(1 - \frac{w/c}{w/c + \rho_w/\rho_c} \right) \alpha_H \tag{5}$$

$$K = (3550\epsilon^{3.6}) \times 10^{-17}; \quad 0.1 \leq \epsilon \leq 0.35 \tag{6}$$



2.5 Final limit-state formulation and solution method

The final LS function is obtained by modeling the capacity function, $C(\mathbf{x})$ or hardened paste tensile strength, on the order of 6–9% of the total compressive strength based upon an empirical fit [24]. To assess the exposure categories and design criteria, the LS function shown in Eq. 7 is derived where the compressive strength, f_c , total entrained air content, A , and spacing factor, \bar{L}_h , are the random variables of interest. Figure 4 displays an analytic output for Eq. 7, where the zero value contour line defines the region of failure where $D(\mathbf{x})$ exceeds $C(\mathbf{x})$.

$$LSF(f_c, \bar{L}_h, A) = 100 + 0.057(f_c) - 0.03\eta \frac{UR\bar{L}_h^2}{K} \left(1.4 \left(\frac{F_p}{A} + 1 \right)^{1/3} + \frac{1}{2} \right) \tag{7}$$

With random distributions defined by ACI, CSA, and BS EN specifications for the design variables, a first-order reliability method (FORM) analysis implementing the improved HL-RF algorithm [19, 25, 26] is used to find the reliability index, β , and associated probability of failure, P_f , of the system. In terms of the presented model, failure can be defined as the likelihood that the hydraulic pressure exceeds the tensile strength of the hardened cement paste. Using the information obtained within the FORM assessment, the relative importance of the selected

design variables can be determined along with the sensitivity of the LS function to the model parameters. Additionally, the results of the system are compared to performance-based measurements, such the durability factor (DF), to validate the model.

3 Experimental database and distributions

3.1 Freeze-thaw data

Similar to previous studies [27, 28], a dataset composed of 85 different ordinary Portland cement (OPC) concrete mixtures was developed from published literature [29–33] where values of A , \bar{L}_h , F_p , and DF, as determined by Procedure A of ASTM C666, were reported. Roughly 50% of the dataset reported the 28-day compressive strength, f_c , of the concrete; those that did not were assigned the mean value of f_c . The dataset represents w/c , total air content, and compressive strength ranging from 0.35 to 0.55, 0.2% to 8.5%, and 20 MPa to 80 MPa, sufficiently bounding the range specified by ACI, CSA, and BS EN for FT resistance. Figure 5 displays the collected data where a DF of 80% demarcates a passing or failing specimen at or before 300 cycles of FT per ASTM C666. In Fig. 5, ranges of w/c are grouped to display that the subsets of the database are well distributed, from a practical standpoint, across A and \bar{L}_h . It is important to note that the freezing rate at which the specimens were tested, aggregate soundness, initial saturation

Fig. 4 Analytic evaluation of the developed LS function where the compressive strength is assumed as 27.6 MPa (4 ksi), over a domain of A and \bar{L}_h

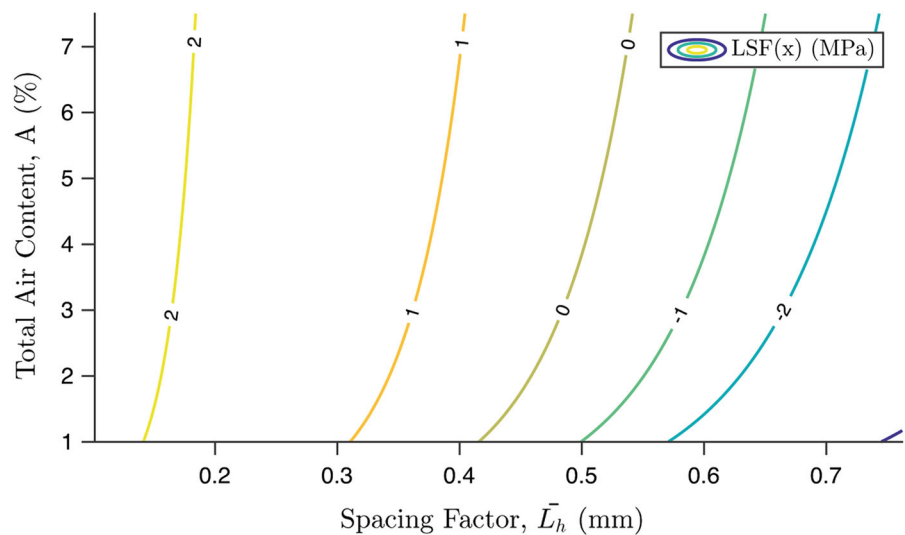
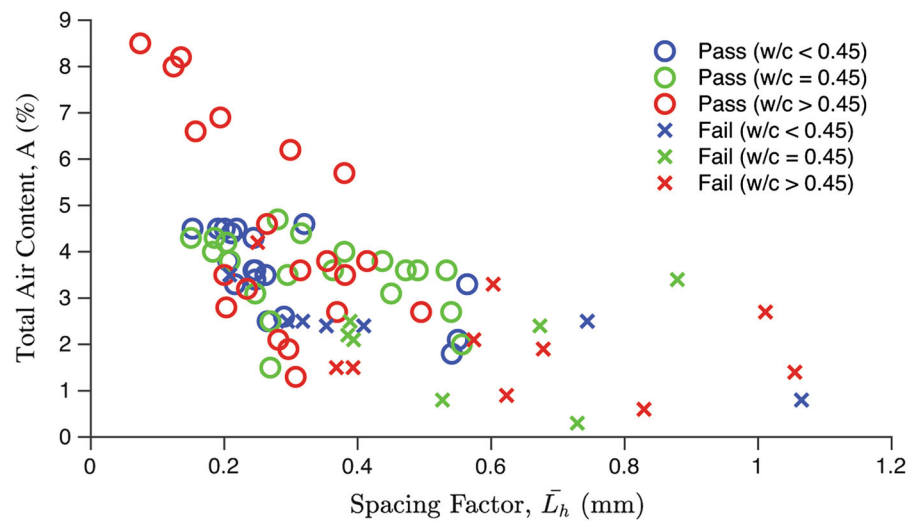


Fig. 5 Cumulative ASTM C666 test results for concretes with w/c ranging from 0.35 to 0.55



conditions, and the specimen-curing period were not collectively reported.

Due to the fact that the studies represented in the FT database were conducted from 1981 to 2012, modifications to ASTM C666 were reviewed to ensure the data could be collectively evaluated. It was found that only minor changes were made to the test method since 1977 [25, 34], so the data are comparable. The ranges of material parameters, such as for f_c , A , and \bar{L}_h , from the respective studies [i.e., 29–33] were found to represent the full domains of interest for each parameter for the presented limit-state model and analysis.

3.2 Random variable distributions and international exposure categories

For the purposes of exposure category and experimental assessment, the design variables are treated as statistically independent, and each is assumed to have a lognormal distribution. Due to the fact that the hydraulic pressure theory singularly assesses the hardened cement paste shell matrix around an air void, the tensile strength of the paste is correlated with the gel-space ratio rather than the total air content [13]. Similarly, it has been experimentally displayed that the relationship between the spacing factor and the total entrained air content is too scattered to draw a meaningful conclusion in terms of correlation and is further complicated without knowledge of admixture combination [27, 35]. For example, based upon Fig. 5, a concrete mixture with a measured spacing factor of

0.4 mm can have a measured total air content ranging from 1.5 to 6%. Similar trends were found in [27] and also displayed that variations in total air content and spacing factor for the same mixture after re-tempering were uncorrelated.

Due to the fact that the lognormal distribution is skew-right, or contains more probability content at greater values as compared to a normal distribution, the design specifications are either under- or over-estimated. For example, per ACI 201.2R-16 and under an F2 exposure, the concrete compressive strength is required to have a minimum average strength of 25 MPa (3500 psi) prior to initial exposure to freeze-thaw cycling [12]. The design strength would be higher than 25 MPa, substantiating the lognormal distribution and resulting in an over-estimated reliability. The defined air content would have the same effect, whereas the skew-right nature of the spacing factor distribution would result in an under-estimation of the reliability of the system. Further justification of the use of a lognormal distribution for the spacing factor is obtained by the published distributions of air voids using standard ASTM C457 techniques in 2012 by Liu and Hansen [36].

With the distribution functions established, means and standard deviations can be obtained by the provisions for concrete FT resilience found in ACI, CSA, and BS EN codes and committee documents. Table 1 summarizes the exposure categories for each organization excluding the exposures for combined FT and deicing salt exposures. The values specified by ACI committee 201 are utilized for the exposure

Table 1 Summary table of international design provisions for concrete exposed to FT [9–12]

Severity (units)	Exposure category	Max. w/c	Min. f_c at 28 days		Total air content ^b (%)	Min. cement content		Air void parameter, \bar{L}	
			(MPa)	(ksi)		($\text{kg} * \text{m}^{-3}$)	($\text{lb} * \text{cy}^{-1}$)	(mm)	(in)
Moderate (low chance of saturation)	ACI 318—F1	0.55	24	3.5	5.0 ^c	—	—	—	—
	CSA—F2	0.55	25	3.6	4–7	—	—	—	—
	BS EN—XF1	0.55	30	4.4	—	300	500	—	—
	ACI 201—F1	0.50	25 ^a	3.6	6.5 ^c	—	—	—	—
Severe (high chance of saturation)	ACI 318—F2	0.45	31	4.5	6.0 ^c	—	—	—	—
	CSA—F1	0.50	30	4.4	5–8	—	—	0.23 ^e	0.09 ^e
	BS EN—XF3	0.50	30	4.4	$\geq 4.0^d$	320	540	—	—
	ACI 201—F2	0.45	25 ^a	3.6	7.0 ^c	—	—	—	—

^aACI 201 specifies their min. f_c as the average compressive strength value prior to exposed to a single FT cycle

^bTotal air content values for concrete mixtures with a maximum aggregate size near 19.1 mm (0.75 in)

^cACI 318 and 201 allow $\pm 1.5\%$ departure on of the specified air content

^dBS EN air content is a minimum

^eMinimum allowable value from the average of three measurements

category assessment as the combination of the specified w/c and compressive strengths will provide the most conservative reliability calculation (i.e., as w/c decreases, permeability decreases causing an increase in the estimated hydraulic pressure, accompanied by a lower value of compressive strength).

Significant deviations occur not only in the recommended design values, but also in their definition, as detailed in the footnotes of Table 1. For example, ACI 201 suggests a minimal strength criterion prior to initial exposure to FT where as ACI 318, CSA, and BS EN specify a minimal mean 28-day compressive strength. Additionally, the BS EN codes require a minimal air content, whereas CSA and ACI specify an allowable range for each exposure. Interestingly, CSA requires a minimal \bar{L} for severe exposures using standard ASTM C457 techniques, but ACI and BS EN codes do not adopt any form of required, or suggested, air void parameter.

For purposes of exposure category assessment, a value of 3.4 MPa (500 psi) is adopted for the 2σ value based upon the largest allowable departure in compressive cylinder testing specified in ASTM C39 [37]. ACI 318 and 201 documents [8, 12] allow a 1.5% tolerance for total air content tested on a job site, which is adopted as the 2σ value. It is important to note that design guidelines provide a total air content and the developed model assesses entrained air content.

For the remainder of the paper and calculations, the value of the entrained air content is set equal to the specified total, or fresh, air volume.

Within Chapter 4 of ACI 201.2R-16, it is stated that concrete mixtures with a spacing factor of less than 0.20 mm (0.008 in) perform well in service and under ASTM C666. The chapter further notes that multiple studies have found that mixtures with spacing factors up to 0.36 mm (0.014 in) and as low as 0.10 mm (0.004 in) display high FT resistance. A 2σ deviation of 0.10 mm is selected to accompany the 0.20 mm (0.008 in) mean.

4 Results and discussion

4.1 Exposure category assessments

The values in Table 1 for the ACI 201 F1 and F2 exposure specifications are used as the respective means of the design variable distributions. The degree of cement hydration, α_H , for the 0.5 w/c is set to 0.85 and the 0.45 w/c is set to 0.75 based upon the simple model provided by Bentz in 2005 for sealed curing conditions at 28 days [38]. Paste fractions, established by standard design procedure [39], of either mixture are set to 30% and 31%, respectively. Table 2 details the calculated probability of failure, P_f , for each



Table 2 Probability of failure values for various freezing rates

Exposure category	$R = 11$ ($^{\circ}\text{C h}^{-1}$)	$R = 5$ ($^{\circ}\text{C h}^{-1}$)	$R = 4.4$ ($^{\circ}\text{C h}^{-1}$)
$P_{f,F1}$ (%)	1.22	0.0060	0.0020
$P_{f,F2}$ (%)	1.15	0.0055	0.0018

mixture across the range of allowable freezing rates per ASTM C666.

As displayed, the P_f values for the F1 exposure category are slightly larger than those found for the F2 exposure for each freezing rate. This finding is expected due to the reductions in mean air content and estimated permeability associated with the F1 exposure category, which effectively increase the hydraulic pressures on the solid matrix during freezing while keeping the distribution of spacing factor and compressive strength the same. Interestingly, the values in Table 2 display a three order of magnitude difference in probability of failure from the largest to smallest allowable freezing rate. As most, if not all, experimental studies do not publish the freezing rate used in their experiments, significant variability is introduced when validating the LS function with ASTM C666 data as displayed by the results of the reliability assessment in Table 2. For the remaining calculations, a freezing rate, R , of $5^{\circ}\text{C} \cdot \text{h}^{-1}$ is used following [7], but could be changed to evaluate the resistance of a concrete placement if the freezing rate of the site condition is known.

4.2 Importance and sensitivity study

Order of importance and sensitivity analyses enable assessment of the influence of the design variables and LS function model parameters on system reliability. The standard importance vector for the F2 exposure variable distributions and explicit inputs is shown in Table 3. The importance vector measures the respective contribution of the design variable to variance in

Table 3 Standard importance vector

Random variable importance values		
f_c	\bar{L}_h	A
- 0.0378	0.9991	- 0.0193

the LS function, providing a relative measure of variable importance. Comparing the importance values for each random variable in Table 3, the value for the spacing factor is over an order of magnitude larger than the compressive strength and entrained air content values. This result indicates that \bar{L}_h dictates the response of the system undergoing FT. From the signs of the importance values, increasing compressive strength and air content increases reliability as expected, while increasing the spacing factor decreases reliability. Based on the importance values, it is concluded that the probability of failure contours are governed by the spacing factor. Figure 6 shows the relationship—the probability of failure is strongly dependent upon the spacing factor for values of 0.25 mm (0.010in) and greater.

The scaled importance vectors, $\bar{\delta}$ and $\bar{\eta}$, describe sensitivities of the reliability index, β , with respect to the variable means and standard deviations, respectively. Scaling enables comparison of the random variables across distributions, units, and scales, with the sensitivities quantifying the effect of changes in the means or standard deviations on the reliability. Table 4 details the scaled importance vectors. Again, it was found for both scaled importance vectors that the spacing factor, \bar{L}_h , influences β the most followed by the compressive strength. From Table 4, decreasing the mean of the spacing factor distribution will increase the overall reliability of the system.

Sensitivities for the LS function model parameters are also investigated to gain a better physical understanding of the influence of components of the model on the reliability of the system. Table 5 provides the sensitivities for the seven parameters, where $\nabla\beta$ indicates the change in reliability index, β , given a unit change in the parameter. The last row of Table 5, $\Delta\beta$, displays the expected change in β for a 5% reduction in the initial value used in the F2 exposure category assessment calculation for parameters S_{fc} , η , S_{cp} , U , and p_f . The $\Delta\beta$ values shown for R and K were resolved from a reduction in the freezing rate by 1°C



Fig. 6 Probability of failure assessment for variable means of A and \bar{L}_h within allowable range specified by ACI provision 201.2R-2016

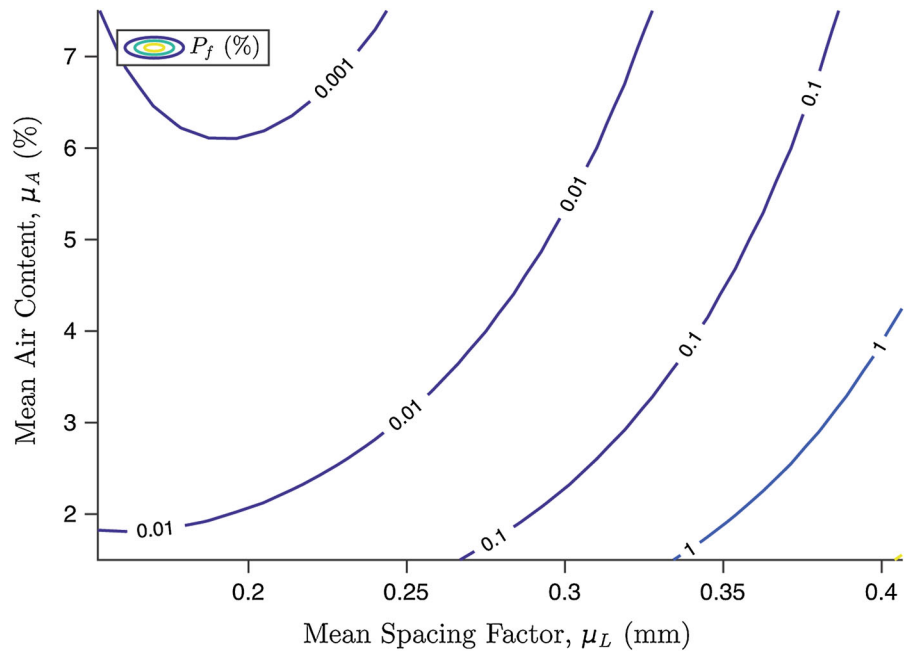


Table 4 Scaled importance vectors

Importance vector	Random variable importance values		
	f_c	\bar{L}_h	A
$\bar{\delta}$ (means)	0.0384	- 0.1376	0.0198
$\bar{\eta}$ (deviations)	- 0.0082	- 3.5072	- 0.0035

per hour and an increase in the degree of cement hydration by 5%.

Considering the value of capillary saturation in Powers’ model, S_{cp} , is bound from 0.917 to 1, the influence it has on the outcome of β is substantial. The only other factors that influence the paste-void system on the same order of magnitude are the permeability, K , and freezing rate, R . Clearly, small changes in the

inputs for K , which is written as a function of the w/c and α_H , results in a substantial change in the reliability of the system. Similarly, the influence of the model with respect to change in freezing rate, R , as demonstrated by the exposure category assessment, is substantial.

4.3 Experimental comparison and validation

To assess the model, a comparison with experimental data is conducted. Average values of design variables and model parameters are determined from the FT dataset values and used to find the probability of failure, P_f , over the same domain of total air content and spacing factor shown in Fig. 5. Figure 7 shows the total FT dataset overlaid on the calculated database-mean P_f contour lines. In the figure, the model and

Table 5 LS function model parameter β sensitivities

Sensitivity	LS function parameter						
	S_{fc}^a	η	S_{cp}	U	R	K	p_f
Initial value	0.057	0.019	1	0.232	1.39e-3	6.94e-17	31.0
$\nabla\beta$	9.294	- 42.040	- 8.875	- 3.443	- 575.480	1.15e16	- 0.006
$\Delta\beta$	- 0.026	0.040	0.444	0.0399	0.1599	- 0.3616	0.009

^a S_{fc} denotes the slope of the tensile strength capacity function, $D(\mathbf{x})$



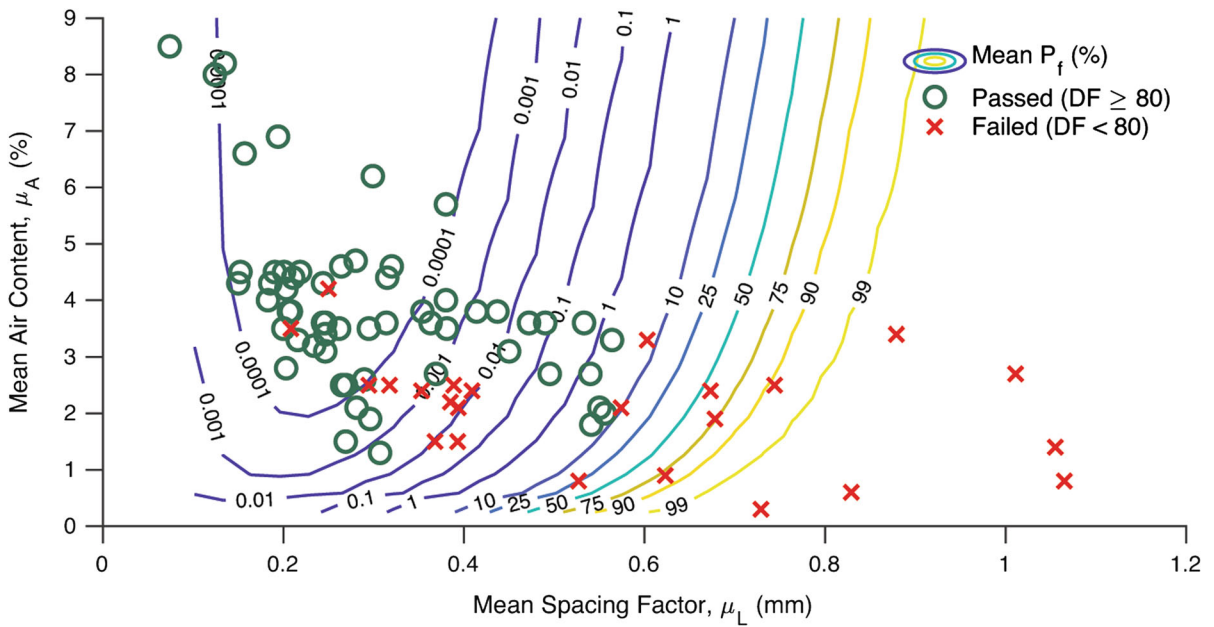


Fig. 7 Cumulative FT data overlaid on the mean P_f contour for average values from the FT database [27–31]

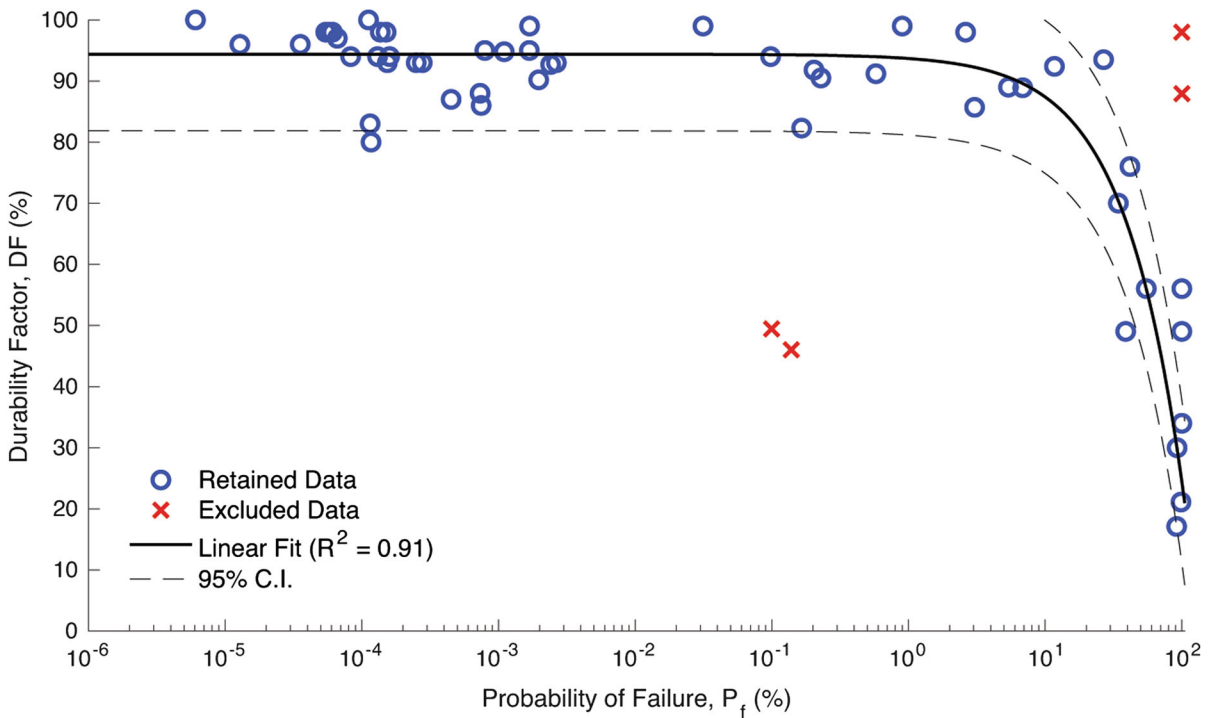


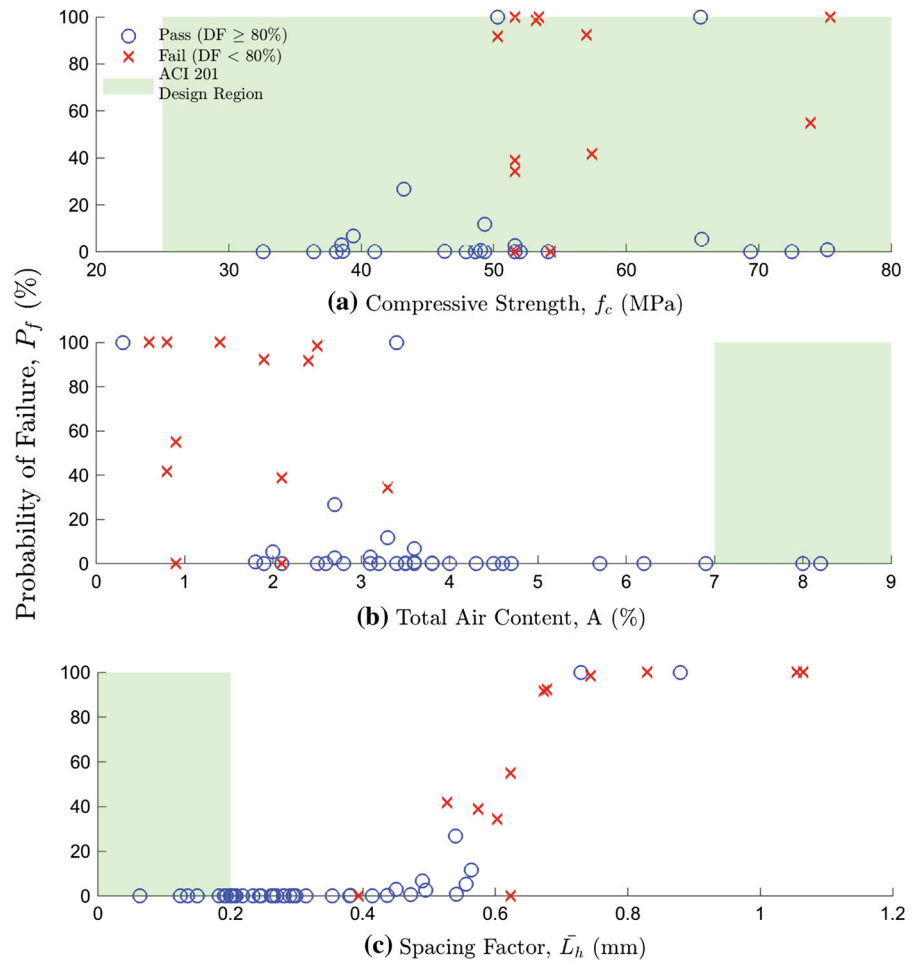
Fig. 8 Cumulative analysis of developed LS function to predict performance by experimental assessment [27–31]

experimental data follow a comparable trend—as air content decreases and spacing factor increases, failure is more likely to occur. It is important to note that

Fig. 7 only directly displays the influence of two variables (i.e., A and L) on the mean P_f contour and therefore provides a limited perspective on the overall



Fig. 9 Comparison of design variables \bar{L}_h , A , and f_c to P_f , ACI 201 design recommendations, and passing or failing ASTM C666 for the cumulative FT dataset [12, 27–31]



utility of the derived limit-state function. For example, it can be clearly seen that a cluster of failing specimens is within the 0.001 and 0.01 mean P_f contours—this is attributed to the fact that the mean P_f here is not representative for those specific mixtures as it does not consider their respective values of f_c , w/c , or F_p .

To validate the model, each value of design variable and model parameter associated with a test specimen is analyzed using FORM and the developed LS function to determine an associated P_f . Figure 8 displays the linear trend found between the calculated values of P_f and their reported DF using a bisquare weighting method that deletes extreme outliers and down-weights mid-outliers. Figure 9 shows the relationship between the P_f of each test specimen and its reported spacing factor, compressive strength, and total air content, while contrasting the ability for ACI 201 design guidance and the probabilistic model to

predict performance under ASTM C666. It is clear that the relationship between spacing factor and reliability is strongest and that the total air content and compressive strength, despite being specified design variables, displays significant scatter when compared to P_f . Furthermore, Fig. 9 shows that the probabilistic model can easily discriminate between passing and failing ATSM C666 specimens, whereas ACI 201 design guidance cannot.

To find the relationship between \bar{L}_h and P_f , a simple exponential equation with the form $P_f(\bar{L}_h) = C_1 e^{C_2 \bar{L}_h}$, where C_1 and C_2 are constants, is fit to the data using the same bisquare weighting method and least squares. Equation 8 provides the exponential function found and Fig. 10 shows the curve overlaid on the FT data. An exponential equation was selected, rather than cubic root, to capture the initial exponential gain in probability of failure with increasing spacing factor.



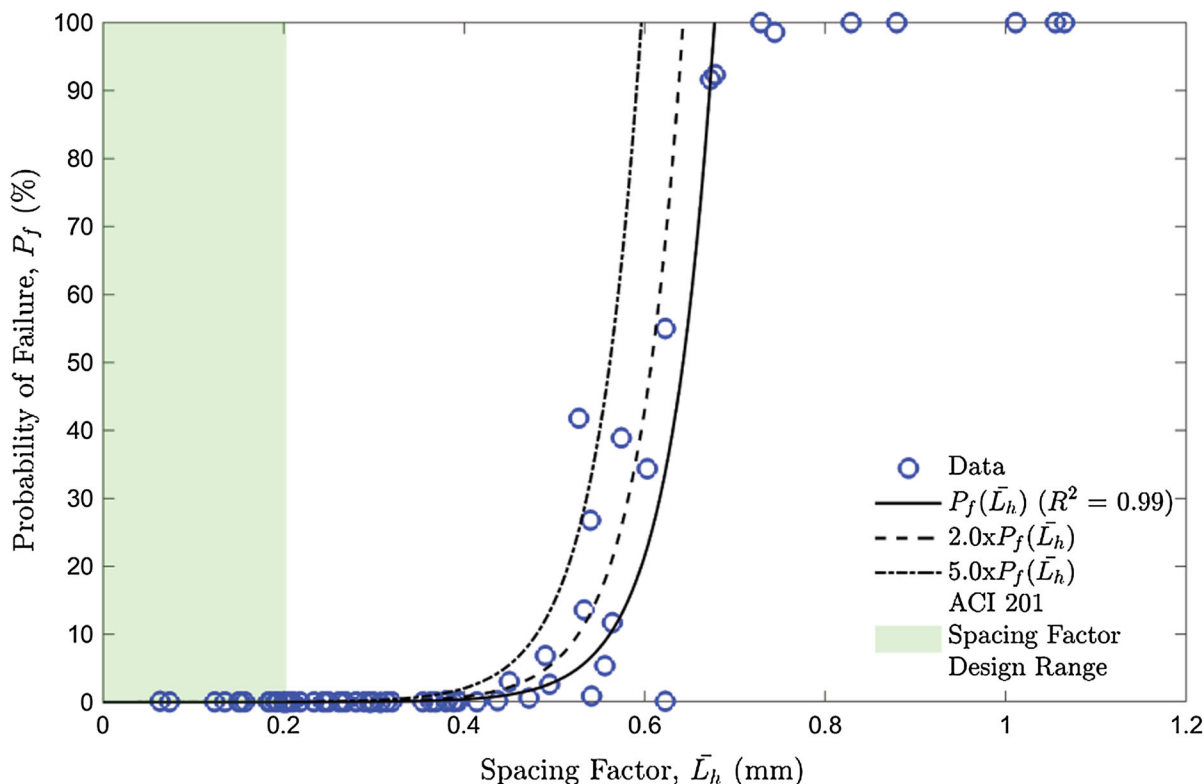


Fig. 10 Exponential function development for probabilistic design of air-entrained concrete [12, 27–31]

Figure 10 also depicts two exponential fits where the values of Eq. 8 have been multiplied by 2 and 5, representing factors of safety to be used for design purposes. Both the experimental data and $P_f(\bar{L}_h)$ equation show the range of spacing factors that is known to perform well under FT exposure during ASTM C666 testing [i.e., ranging from 0.10 mm (0.004 in) to 0.36 mm (0.014 in)]. For \bar{L}_h greater than 0.36 mm (0.014 in), the probability of failure begins to significantly increase. These equations enable the design of concrete to meet the desired performance-based specifications for FT resistance.

$$P_f(\bar{L}_h) = 1.44 \times 10^{-4} e^{19.5\bar{L}_h} \quad (8)$$

5 Conclusions

Through the use of the developed LS function, the following conclusions are drawn:

1. The spacing factor, \bar{L}_h , has the largest influence on concrete FT performance, as assessed through accelerated testing. Although the probability of failure values for the ACI 201 FT exposure categories were reasonably low, even for the highest freezing rate considered, spacing factor is not currently specified within ACI or BS EN codes. It should be recalled that the spacing factor distribution used in the exposure category assessment was based on values that have been shown to perform well under controlled laboratory testing.
2. The saturation state, freezing rate, and permeability significantly influence the concrete FT response, as shown by the sensitivity assessment. Despite the fact that the freezing rate in the field cannot be directly controlled, the permeability of the concrete can be designed through selection of an appropriate w/c , inclusion of supplementary cementitious materials, and ensuring adequate curing periods.
3. A critical saturation state, where exposure to a single FT cycle results in measurable loss in modulus, likely corresponds to a value of Powers'

spacing factor near, or above, 0.5 mm (0.020 in) where the probability of failure asymptotically increases. This finding displays that the resistance of concrete to FT is significantly dependent upon the initial geometry of the entrained air void system.

Lastly, a key contribution of the developed LS function is a simple exponential equation that can be used to inform air-entrained concrete mixture design or to carry out predictive reliability assessments of in-place concrete. The functions shows that as the spacing factor increases past a value of 0.5 mm there is a exponential increase in probability of failure of the concrete. It should be noted that the presented work does not analyze or consider the influence of deicing salts, which categorizes the very severe exposures for FT in ACI, CSA, and BS EN codes, and only considers OPC concretes. The presented work displays that the spacing of the air voids is more important than the total volume of the entrained air through the presentation of a probabilistic model that can be readily used by design engineers and manufacturers.

Acknowledgements This material is based upon work support under a Department of Energy, Office of Nuclear Energy, Integrated University Program Graduate Fellowship. The authors would also like to acknowledge the ACI Concrete Research Council for their interest and support for modernizing of freeze-thaw design provisions.

Funding The only funding source received was a graduate fellowship provide to author Scott Smith from the Department of Energy, Office of Nuclear Energy, Integrated University Program. Any opinions, findings, conclusions or recommendations expressed in this publication are those of the author(s) and do not necessarily reflect the views of the Department of Energy Office of Nuclear Energy.

Compliance with ethical standards

Conflict of interest The authors declare that they have no conflicts of interest.

Ethical standards The authors declare that they have complied with ethical standard of work.

Appendix: Notation list

- A : Total entrained air content (%)
- α_H : Degree of cement hydration (%)
- β : Reliability index.

- DF : Measurement ASTM C666 Durability Factor (%)
- ϵ : Paste capillary porosity (Volume fraction).
- f_c : Concrete compressive strength (MPa).
- F_p : Paste fraction of concrete mixture (Volume fraction).
- K : Permeability of saturated, hardened cement paste (cm^2).
- L : Approximate thickness of hardened cement paste shell (m).
- \bar{L} : ASTM C457 Powers' spacing factor.
- \bar{L}_1 : Powers' spacing factor for p_f/A less than 4.32.
- \bar{L}_h : Powers' spacing factor for p_f/A greater than 4.32.
- μ : Distribution mean.
- η : Viscosity of water near 0 °C, Pa * s.
- P_f : Probability of failure, (%)
- $P_f(\bar{L}_H)$: Probability of failure function (%), \bar{L}_H has units of millimeters.
- U : Weight of water present per volume of cement paste, ($\text{kg} * \text{°C}^{-1}$).
- R : Freezing rate, ($\text{°C} * \text{h}^{-1}$).
- r_b : Radius of entrained air void, (m).
- ρ_c : Density of cement, ($\text{kg} * \text{m}^{-3}$).
- ρ_w : Density of water, ($\text{kg} * \text{m}^{-3}$).
- S_{cp} : Saturation of paste capillary porosity.
- S_{fc} : Slope of the tensile strength model.
- σ : Distribution standard deviation.

References

1. Klieger P (1952) Studies of the effect of entrained air on the strength and durability of concretes made with various sizes of aggregates. Proc Highw Res Board 31:177–201
2. Klieger P (1956) Curing requirements for scale resistance of concrete. Highw Res Board Bull 150:18–31
3. Weiss WJ (2015) Concrete pavement joint durability: a sorption based model for saturation, the role of distributed cracking and calcium oxychloride formation. In: 10th international conference on mechanics and physics of creep, shrinkage, and durability of concrete and concrete structures. <https://doi.org/10.1061/9780784479346.025>
4. Li W, Pour-Ghaz M, Castro J, Weiss WJ (2012) Water absorption and critical degree of saturation relating to freeze-thaw damage in concrete pavement joints. J Mater Civ Eng 24:299–307. [https://doi.org/10.1061/\(ASCE\)MT.1943-5533.0000383](https://doi.org/10.1061/(ASCE)MT.1943-5533.0000383)
5. Lucero CL, Bentz DP, Hussey DS, Jacobsen DL, Weiss WJ (2015) Using neutron radiography to quantify water transport and the degree of saturation in entrained air cement



- based mortar. *Phys Procedia* 69:542–550. <https://doi.org/10.1016/j.phpro.2015.07.077>
6. Moradillo MK, Ley MT (2017) Quantitative measurement of the influence of degree of saturation on ion penetration in cement paste by using X-ray imaging. *J Constr Build Mater* 141:113–129. <https://doi.org/10.1016/j.conbuildmat.2017.03.007>
 7. Mayercsik NP, Vandamme M, Kurtis KE (2016) Assessing the efficiency of entrained air voids for freeze-thaw durability through modeling. *J Cem Concr Res* 88:43–59. <https://doi.org/10.1016/j.cemconres.2016.06.004>
 8. Cavalline TL, Ley MT, Sutter LL, Weiss WJ, Van Dam TJ (2016) A road map for research and implementation for freeze-thaw resistant highway concrete. In: 11th international conference on concrete pavements
 9. 318 ACI (2014) 318-14: building code requirements for structural concrete and commentary. American Concrete Institute, Farmington Hills
 10. CSA (2014) A23.1-14/A23.2-14: concrete materials and methods of concrete construction/testing methods and standard practice for concrete. Canadian Standard Association, Mississauga
 11. BS EN (2000) Concrete—part 1: specification, performance, production and conformity. British Standards Institution, London
 12. 201 ACI (2016) Guide to durable concrete (ACI 201.2R-16). American Concrete Institute 2016
 13. Powers TC (1949) The air requirement of frost-resistant concrete. In: Proceedings of the highway research board, vol 29
 14. Powers TC, Brownyard TL (1947) Studies of the physical properties of hardened portland cement paste. *J Am Concr Inst* 43:101–132, 249–336, 469–505, 549–602, 669–712, 845–880, 933–992
 15. Cho T (2007) Prediction of cyclic freeze-thaw damage in concrete structure based on response surface method. *Constr Build Mater* 21:2031–2040. <https://doi.org/10.1016/j.conbuildmat.2007.04.018>
 16. Cho T (2010) Prediction of cyclic freeze-thaw damage in concrete structures based on an improved response surface method. *Int J Railw* 3:7–13. <https://doi.org/10.1016/j.conbuildmat.2007.04.018>
 17. Chen F, Qiao P (2015) Probabilistic damage modeling and service-life prediction of concrete under freeze-thaw action. *J Mater Struct* 48:2697–2711. <https://doi.org/10.1617/s11527-014-0347-y>
 18. Wawrzęczyk J, Molendowska A (2017) Evaluation of concrete resistance to freeze-thaw based on probabilistic analysis of damaged. *Procedia Eng* 193:35–41. <https://doi.org/10.1016/j.proeng.2017.06.183>
 19. Hasofer AM, Lind NC (1975) Exact and invariant second-moment code format. *J Eng Mech Div* 100:111–121
 20. Hover KC, Bickley J, Hooten RD (2008) Guide to specifying concrete performance: phase II report of preparation of a performance-based specification for cast-in-place concrete. RMC Research and Education Foundation
 21. Pigeon M, Pleau R (1995) Theories of frost action and deicer salt scaling mechanisms. In: Bentur A, Mindess S (eds) *Durability of concrete in cold climates*, 1st edn. Taylor and Francis, London, pp 12–23
 22. Coussy O, Monteiro P (2008) Poroelastic model for concrete exposed to freezing temperatures. *J Cem Concr Res* 38:40–48. <https://doi.org/10.1016/j.cemconres.2007.06.006>
 23. ASTM (2015) ASTM C666/C666M-15 standard test method for resistance of concrete to rapid freezing and thawing. ASTM International. https://doi.org/10.1520/C0666_C0666M-03
 24. Gonnerman HF, Shuman EC (1928) Compression, flexure, and tension tests of plain concrete. *Proc Am Soc Test Mater* 28:527
 25. Rackwitz R, Fiessler B (1978) Structural reliability under combined random load sequence. *J Comput Struct* 9:489–494. [https://doi.org/10.1016/0045-7949\(78\)90046-9](https://doi.org/10.1016/0045-7949(78)90046-9)
 26. Zhang Y, Der Kiureghian A (1995) Two improved algorithms for reliability analysis. Reliability and optimization of structural systems. In: Proceedings of the 6th IFIP WG 7.5 working conference on reliability and optimization of structural systems
 27. Saucier F, Pigeon M, Cameron G (1991) Air void stability, part V: temperature, general analysis and performance index. *ACI Mater J* 88(1):25–26
 28. Attiogbe EK, Nmai CK, Gay FT (1992) Air-void system parameters and freeze-thaw durability of concrete containing superplasticizers. *ACI Concr Int* 68:57–61
 29. Yamato T, Emoto Y, Soeda M (1986) Strength and freezing-and-thawing resistance of concrete incorporating condensed silica fume. *Am Concr Inst Spec Publ* 91:1095–1118
 30. Okada E, Hisaka M, Kazama Y, Hattori K (1981) Freeze-thaw resistance of superplasticized concretes. *Am Concr Inst Spec Publ* 68:215–232
 31. Pigeon M, Pleau R, Aitcin P (1986) Freeze-thaw durability of concrete with and without silica fume in ASTM C 666 (procedure A) test method: internal cracking vs. scaling. *Cem Concr Aggreg* 8:76–85. <https://doi.org/10.1520/CCA10060J>
 32. Felice RV (2012) Frost resistance of modern air entrained concrete mixtures. Masters Thesis Oklahoma State University
 33. Tanesi J, Meininger R (2006) Freeze-thaw resistance of concrete with marginal air content. US Department of Transportation Federal Highway Administration
 34. ASTM (1997) ASTM C666—77 (historical version) standard test method for resistance of concrete to rapid freezing and thawing. American Society for Testing and Materials, ASTM International
 35. Felice R, Freeman JM, Ley MT (2014) Durable concrete with modern air-entraining admixtures. *ACI Concr Int* 36:37–45
 36. Liu Z, Hansen W (2016) A geometrical model for void saturation in air-entrained concrete under water exposure. *J Constr Build Mater* 124:475–484. <https://doi.org/10.1016/j.conbuildmat.2016.07.113>
 37. ASTM (2017) ASTM C39/C39M—17 standard test method for compressive strength of cylindrical concrete specimens. *Am Soc Test Mater ASTM Int*. https://doi.org/10.1520/C0039_C0039M-17
 38. Bentz DP (2006) Influence of water-to-cement ratio on hydration kinetics: simple models based on spatial considerations. *J Cem Concr Res* 36:238–244. <https://doi.org/10.1016/j.cemconres.2005.04.014>
 39. Kosmatka SH, Wilson ML (2016) Design and control of concrete mixtures, 16th edn. Portland Cement Association, New York

